

## Temperature distribution of ceramic panels of a V94.2 gas turbine combustor under realistic operation conditions

Mohammad Javad Namayandeh<sup>1,2</sup>,  
Mehdi Mohammadimehr<sup>\*1</sup> and Mojtaba Mehrabi<sup>1,3</sup>

<sup>1</sup> Department of Solid Mechanics, Faculty of Mechanical Engineering, University of Kashan, Kashan, Iran

<sup>2</sup> Mechanical Expert of Combined Cycle Power Plant, Kashan, Iran

<sup>3</sup> Department of Mechanics, Faculty of Engineering, University of Isfahan, Isfahan, Iran

(Received February 7, 2019, Revised May 29, 2019, Accepted August 18, 2019)

**Abstract.** The lifetime of a gas turbine combustor is typically limited by the durability of its liner, the structure that encloses the high-temperature combustion products. The primary objective of the combustor thermal design process is to ensure that the liner temperatures do not exceed a maximum value set by material limits. Liner temperatures exceeding these limits hasten the onset of cracking which increase the frequency of unscheduled engine removals and cause the maintenance and repair costs of the engine to increase. Hot gas temperature prediction can be considered a preliminary step for combustor liner temperature prediction which can make a suitable view of combustion chamber conditions. In this study, the temperature distribution of ceramic panels for a V94.2 gas turbine combustor subjected to realistic operation conditions is presented using three-dimensional finite difference method. A simplified model of alumina ceramic is used to obtain the temperature distribution. The external thermal loads consist of convection and radiation heat transfers are considered that these loads are applied to flat segmented panel on hot side and forced convection cooling on the other side. First the temperatures of hot and cold sides of ceramic are calculated. Then, the thermal boundary conditions of all other ceramic sides are estimated by the field observations. Finally, the temperature distributions of ceramic panels for a V94.2 gas turbine combustor are computed by MATLAB software. The results show that the gas emissivity for diffusion mode is more than premix therefore the radiation heat flux and temperature will be more. The results of this work are validated by ANSYS and ABAQUS softwares. It is showed that there is a good agreement between all results.

**Keywords:** V94.2 gas turbine combustor; combustion chamber; temperature distribution; realistic operation conditions; 3D-FDM

### 1. Introduction

Gas turbines in simple-cycle mode have long been used by utilities for limited peak power generation. Moreover, industrial facilities use gas turbine units for on-site power generation, usually in combination with process heat production such as process steam and hot water (Poullikkas 2005). The use of gas turbines for generating electricity dates back to 1939. In the last decades, gas turbines have become the power generation technology of choice (Rajaei *et al.* 2017),

---

\*Corresponding author, Associate Professor, E-mail: [mmohammadimehr@kashanu.ac.ir](mailto:mmohammadimehr@kashanu.ac.ir)

due mainly to their low emissions, low capital costs and high efficiencies (Termaath *et al.* 2006, Koc 2015). Also, these turbines are one of the most widely-used power generating technologies which power density and efficiency of them have increased drastically. Due to considerable investments in research and development, the performance of industrial gas turbines has been improved, in terms of plant capacity, reliability, fuel-to-electricity conversion efficiency and availability (Najjar 2000). The improved gas turbines for power generation have reached thermal efficiencies close to 40% at net power outputs beyond 270 MW. The greater availability of fuel resources, such as natural gas, the significant reduction in capital costs and the introduction of advance cycles, have also been a success factor for the increased deployment of gas turbines for base load applications. The improvements are primarily a result of increased thermodynamic parameters like pressure ratio and turbine inlet temperature (combustor exit temperature). Both parameters have direct impact on the heat load and hence the net power output. The effect of various parameters such as hydrogen content, combustor air pressure, fuel/air ratio, the gas temperature on the gas heat radiation, also total heat transfer on the different combustion chamber types are investigated in some literatures.

In order to consider the effect of a certain load profile on the overall lifetime of the combustion hardware, especially the combustion liner, Matarazzo and Laget (2011) examined the impact of the changes in the operational parameters on the temperature and heat flux at the liner surface. Kim *et al.* (2010a) investigated the failure analysis and the lifetime prediction from distributions of temperature and thermal stress in after shell section of gas turbine can-combustion liner. They divided combustor liner into three sections of forward shell, center shell and after shell and used a numerical simulation using the finite element method (FEM) and finite volume method (FVM) to calculate distributions of temperature and thermal stresses in the liner. Also, they (Kim *et al.* 2010b) studied conjugated heat transfer to obtain temperature distributions in a combustion liner with six combustion nozzles. Bradshaw and Waitz (2006) presented a probabilistic framework for quantifying the impact of manufacturing variability on combustor liner life. Wan *et al.* (2019) considered an experimental study on the temperature decay profile of ceiling jet by two propane flames burning under an unconfined ceiling. Some researchers worked about the thermal effect on various structures including double-walled boron nitride nanotubes (Arani *et al.* 2012a), nanocomposite cylinder (Arani *et al.* 2012b), nanorod (Mohammadimehr and Rahmati 2013), sandwich plate (Mohammadimehr and Mostafavifar 2016), double-bonded sandwich microplate (Mohammadimehr *et al.* 2017), microbeam (Rostami *et al.* 2018), hollow circular plate and sandwich plate (Mohammadimehr *et al.* 2018a, b). Yang *et al.* (2017) presented a theoretical analysis to study the contribution of wall emission and wall reflection to the incident radiation measured by radiometers. They developed a simplified radiation model considering the non-homogeneous gas-particle medium inside the combustor as a gray surface with uniform properties which radiates with the same emissive power as the medium. Wang *et al.* (2019) devised thermal protection systems (ITPS) with single layer metal and multilayer ceramic matrix composite cellular sandwich panel and established thermal insulation effect and risk of buckling failure. They calculated transient heat transfer characteristics based on numerical approaches and showed that ITPS with specific graded insulation materials can present lower temperature and better temperature distribution uniformity than those of ITPS filled with uniform insulation material. Sanaye *et al.* (2018) presented an integrated plant for production of combined cooling, heating, power and water (CCHPW) included a gas turbine, an HRSG producing steam and absorption refrigeration system. Mukherji *et al.* (2012) development Co-Re alloy new materials for gas turbines used at temperatures considerably higher than single crystal Ni-based superalloys. Chau *et*

*al.* (2017) employed high-pressure gas atomization to prepare the Fe-based  $\text{Fe}_{50}\text{Cr}_{24}\text{Mo}_{21}\text{Si}_2\text{B}_3$  alloy powder. They studied effects of flow rate of atomizing gas on the median powder diameter and showed that the powder size reduced by increasing the flow rate of atomizing gas. Perpignan *et al.* (2018) investigated the various definitions of the flameless combustion (FC) regime and demonstrated that modelling of the FC regime is still not capable of predicting intermediate species and pollutant emissions. Sousa *et al.* (2017) provided a numerical tool to evaluate precisely the thermodynamic and non-isentropic processes across the entire engine and pressure ratios for which the rotating detonation based on engine outperforms the conventional power plants based on the Brayton cycle. Aditya *et al.* (2019) created a three-dimensional direct numerical simulation (DNS) for a turbulent hydrogen-air flame, represented with detailed chemistry, stabilized in a model gas-turbine combustor. They showed that when the flame is stabilized at its design position, combustion occurs due to both autoignition and flame propagation (deflagration) modes at different locations within the combustion chamber. Rist *et al.* (2017) considered the economic dispatch of a single micro-gas turbine under combined heat and power (CHP) operation. They developed partial and full load configurations, an accurate optimization model for solving the economic dispatch problem of integrating the turbine into the grid. Andreini *et al.* (2017) studied the effects of the realistic flow field of a lean burn injector on the adiabatic film cooling effectiveness on an effusion cooled combustor liner using an experimental study dealing with the impact of holes injection angle on the performance of an effusion cooling system. The results of their work demonstrated that the adiabatic film cooling effectiveness maps show a deep impact of the injection angle on the effusion system performance. Martiny *et al.* (1995) calculated evaluated row by row adiabatic film effectiveness and performed flow visualizations on a full coverage film cooling plate with highly inclined holes at different blowing ratios. They illustrated that even with high blowing ratio and therefore with full penetration of jets, an appreciable cooling benefit can be measured in terms of adiabatic film effectiveness. An extensive parametric study realized by Gustafsson and Johansson (2001) where overall cooling effectiveness was tested with Infra-Red thermography. Rahmati and Mohammadimehr (2014) presented vibration analysis of non-uniform and non-homogeneous boron nitride nanorods embedded in an elastic medium under combined loadings. Mohammadimehr *et al.* (2016) considered bending, buckling, and free vibration analysis of MSGT microcomposite Reddy plate reinforced by FG-SWCNTs with temperature- dependent material properties under hydro-thermo-mechanical loadings. Mohammadimehr and Mehrabi (2017) illustrated stability and free vibration analyses of double-bonded micro composite sandwich cylindrical shells conveying fluid flow. Arani *et al.* (2011) worked about dynamic stability of the double-walled carbon nanotube under axial loading embedded in an elastic medium by the energy method. Yazdani *et al.* (2019) presented free vibration of Cooper-Naghdi micro saturated porous sandwich cylindrical shells with reinforced CNT face sheets under magneto-hydro-thermo-mechanical loadings.

The goal of this paper is to evaluate heat transfer and temperature distribution in a V94.2 gas turbine combustor ceramic wall. The combustion chamber wall is heated by radiation and convection from hot gases inside as well as is cooled by radiation and convection to combustor jacket and annulus air outside. To evaluate of the wall temperature distribution, wall adjacent temperatures are required which may be calculated from the wall heat transfer equations. In this section mean temperatures of the hot and cold side of the wall are calculated employing empirical method.

## 2. Model of heat transfer analysis

Gas turbines are essentially composed of three major components: compressor, combustor, and power turbine. The ambient air, as working fluid, is drawn in and compressed by the compressor and directed to the combustor section where fuel is introduced, ignited, and burned to heat the air until the turbine inlet temperature. The hot gases from the combustion chamber are diluted with additional air from the compressor and directed to the power turbine. So, it is clear that the gas turbine performance is highly dependent on the combustion chamber condition. Combustors can either be annular, can-annular, or silo. An annular combustor is a doughnut-shaped, single, continuous chamber that encircles the turbine in a plane perpendicular to the air -flow. Can-annular combustors are similar to the annular; however, they incorporate several can-shaped combustion chambers rather than a single continuous chamber. Annular and can-annular combustors are based on aircraft turbine technology and are typically used for smaller scale applications or lower power. A silo (frame-type) combustor has one or more combustion chambers mounted external to the gas turbine body. Silo combustors are typically larger than annular or can-annular combustors and are used for larger scale applications or higher power. They offer the advantages of simplicity of design, ease of maintenance, and long-life due to low heat-release rates. Fig. 1 shows can-annular and annular combustors configurations from above section.

V94.2 gas turbine is a modern turbine which is widely used for power generation. This model of gas turbine has two silo-type combustion chambers which mounted external to it. An overall view of a V94.2 gas turbine is shown in Fig. 2. In V94.2 gas turbine, the thermal load to the combustor wall is determined by two combustion zones: primary and secondary zones. In the

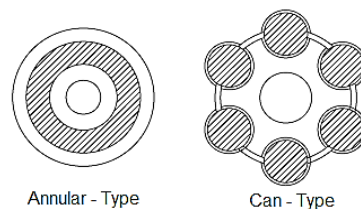


Fig. 1 Can-annular and annular combustors configurations

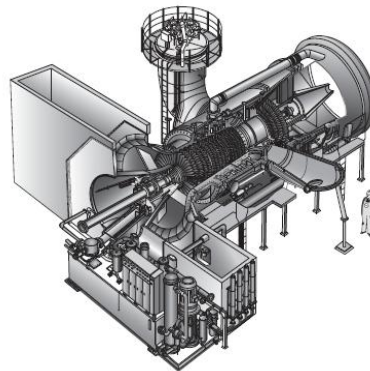


Fig. 2 Overall view of a V94.2 gas turbine

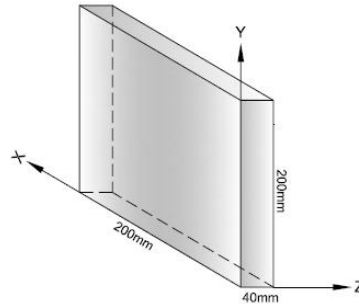


Fig. 3 3D-configuration of ceramic panel

primary zone, the wall heat load is caused by a very hot flame with high radiation and by convection of the combustion hot gases. The radiation heat load with wall is reduced due to the long distance between flame and wall and absorption by the unmixed air. Nevertheless, these flame tube areas are protected using heat resistant alumina panels forming the liner. In secondary zone, the high temperatures of the primary zone are reduced to inlet turbine temperature by adding cold compressor supplied air (called dilution air). Also, flame tube temperature is kept at acceptable level by applying convection cooling to outer surface.

### 2.1 Material model

Ceramic  $200 \times 200 \times 40 \text{ mm}^3$  panels which made of alumina are analyzed with convection and radiation heat load from combustion products on one side, and convective and radiative cooling on the other side. Fig. 3 is the simplified 3D-Configuration of ceramic panel.

### 2.2 Physical and operating condition

In this section, using empirical method, ceramic panels which located on a metallic shell (flame tube), regarded as a container of hot flowing gases, surrounded between the container and the jacket by combustion chamber jacket with air flowing. Generally, the flame tube is heated by radiation and convection from the hot gases inside it, and is cooled by radiation to the jacket and by convection to the annulus air. The relative proportions of the radiation and convection components depend on the operating conditions and geometry. In order to determine the ceramics panel heat transfer boundary conditions, a V94.2 gas turbine is assumed where its compressor supplies air at a pressure of 9.7 bar (9.57 atm) to a combustor at base load. An inlet temperature of 620K (combustion chamber or outlet compressor) is considered, assuming 88% compressor efficiency relative to isentropic compression. Figs. 4-5 show major parts of V94.2 combustion chamber as well as a portion of combustor panel assembly, respectively.

For steady-state condition, the heat transfer into the wall domain in Fig. 5 is balanced by the heat transfer out of it.

$$R_1 + C_1 + K_1 = R_2 + C_2 + K_2 \quad (1)$$

where  $R_1$  and  $R_2$  are the radiation heat flux from the flame and radiation heat flux to the jacket, respectively.  $C_1$  and  $C_2$  denote convection heat flux by hot gas and convection heat flux to annulus

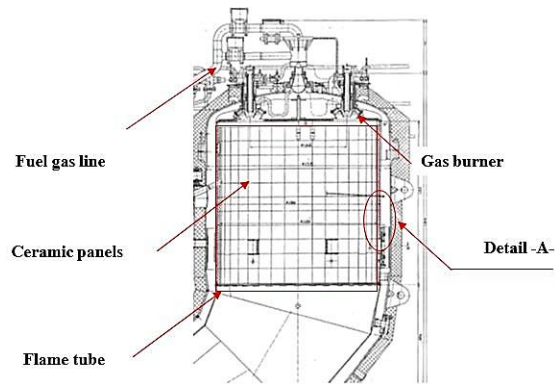


Fig. 4 Major parts of V94.2 combustion chamber

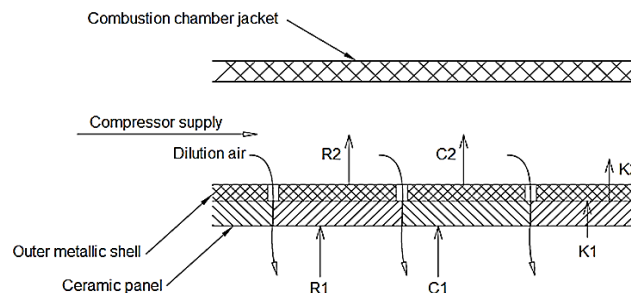


Fig. 5 Combustion chamber assembly (Detail -A-)

Table 1 Summary of actual operating conditions at base load

Inlet compressor temperature ( $T_1$ )	303 K
Outlet compressor temperature ( $T_2$ )	620 K
Inlet compressor pressure ( $P_1$ )	0.890 bar
Outlet compressor pressure ( $P_2$ )	9.7 bar
Inlet turbine temperature ( $T_3$ )	1323 K
Flame temperature ( $T_g$ )	1863 K

air, respectively.  $K_1$  and  $K_2$  illustrate the conduction heat flux through the ceramic panel and the outer metallic shell, respectively.

The used basic assumptions to define the operating environment are listed in Table 1.

### 2.3 Hot side radiation heat flux model

In gas turbine combustors, a significant proportion of the total heat transferred from the combustion gases to the liner is by radiation. Thus, accurate assessments of radiant heat flux are an essential prerequisite for the prediction of liner wall temperatures and liner durability.

Generally, flames work by combining their own carbon molecules with oxygen molecules in

the air to form carbon dioxide. For the generated combustion gases by gas turbine fuels, the total emitted radiation has two types: (1) the “nonluminous” radiation (no soot) that emanates from certain heteropolar gases, notably carbon dioxide and water vapor, and (2) the “luminous” radiation that depends on the number and size of the solid particles (mainly soot) in the flame.

Luminous flames do not get enough oxygen to turn all the carbon that is being burnt into carbon dioxide. Some of this excess carbon is released as soot; that is why luminous flames produce soot, while non-luminous flames do not. Because the non-luminous flames are able to combine all their carbons with oxygen and burn far more efficiently than luminous flames.

The combustion process in gas turbine on natural gas can be classified as diffusion (luminous) and premixed (nonluminous) flame modes, depending on whether the fuel and air are mixed. In the diffusion mode, the fuel/air mixing and combustion take place simultaneously in the flame zone. This generates regions of near -stoichiometric fuel/air mixtures where the temperatures are very high, while in the premixed mode the fuel/air are mixed before combustion. Diffusion flame tend to burn slower and to produce more soot than premixed flame because there may not be sufficient oxidizer for the reaction to go to completion. Thus:

- Premixed flames are short, blue, noisy and the reactions (mixed) are virtually complete.
- Diffusion flames are long, yellow, and quieter and the reactions are incomplete.

In this study, hot side radiation was modeled using equation for radiation from luminous and non-luminous gases.

From Lefebvre the net radiant heat transfer is given by Lefebvre (2010)

$$R_1 = \sigma(\varepsilon_g T_g^4 - \alpha_g T_{w_1}^4) \quad (2)$$

in which  $\sigma$  is the Stefan–Boltzmann constant,  $\varepsilon_g$  is the gas emissivity at flame temperature ( $T_g$ ), and  $\alpha_g$  is the gas absorptivity at wall temperature  $T_{w_1}$ . Both  $\varepsilon_g$  and  $\alpha_g$  are functions of gas composition. However,  $\varepsilon_g$  relates to the emission of radiation from the gas to the wall and depends on  $T_g$ , but  $\alpha_g$  applies to the absorption by the radiation gas from the wall, and hence depends on  $T_{w_1}$ .

In practice, for the effect of absorptivity of the wall surface, the factor  $0.5(1 + \varepsilon_{w_1})$  is introduced. Then (Lefebvre 2010)

$$R_1 = 0.5\sigma(1 + \varepsilon_{w_1})(\varepsilon_g T_g^4 - \alpha_g T_{w_1}^4) \quad (3)$$

where  $\varepsilon_{w_1}$  is the wall emissivity and dependent on the material, temperature and degree of the oxidation of the wall. Gas temperature ( $T_g$ ) is assumed to correspond to an adiabatic flame temperature of 1863 K with a fuel/air ratio (FAR) of 0.022 (TUGA 2012).

Still from Lefebvre (2010), gas absorptivity can be estimated by

$$\alpha_g = \varepsilon_g \left(\frac{T_g}{T_{w_1}}\right)^{1.5} \quad (4)$$

Hence, Eq. (3) may be rewritten as follows (Goodger 2007)

$$R_1 = 0.5\sigma(1 + \varepsilon_{w_1})\varepsilon_g T_g^{1.5} (T_g^{2.5} - T_{w_1}^{2.5}) \quad (5)$$

### 2.3.1 Luminous flames (diffusion)

For luminous flames, gas emissivity  $\varepsilon_g$  is given by Lefebvre (2010)

$$\varepsilon_{g_d} = 1 - \exp[-290P_g L_g (FAR.L_m)^{0.5} T_{g_d}^{-1.5}] \quad (6)$$

where  $P_g$  is the gas pressure in *KPa*,  $L_g$  is the gas luminosity, FAR is the fuel/air ratio and  $L_m$  is the effective radiation beam length in meters.

Gas luminosity is estimated by Lefebvre (2010)

$$L_g = 336 / H^2 \quad (7)$$

where  $H$  is the fuel hydrogen content (by mass) in percent which is calculated from local fuel analysis which is obtained from local gas analysis. The effective radiation beam length  $L_m$  is determined by the size and shape of the gas volume that it is given by the expression (Bergman *et al.* 2011)

$$L_m = 3.6 \frac{V_c}{A_c} \quad (8)$$

in which  $V_c$  and  $A_c$  are the volume and the inside surface of gas container, respectively.

For most practical, the effective radiation beam length for circular cylinder of equal height and diameter (radiation to entire surface) is given by Bergman *et al.* (2011)

$$L_m = 0.6D \quad (9)$$

where  $D$  is the cylinder diameter.

### 2.3.2 Non-luminous flames (premix)

Values of  $\varepsilon_{g_p}$  for non-luminous flames may be obtained from the following approximate formula due to Reeves (1956).

$$\varepsilon_{g_p} = 1 - \exp[-290P_g (FAR.L_m)^{0.5} T_{g_p}^{-1.5}] \quad (10)$$

where  $\varepsilon_{g_p}$  and  $T_{g_p}$  are the gas emissivity for non-luminous flame and flame temperature, respectively.

## 2.4 Hot side convection heat flux model

Of the total heat transfer processes that determine the liner temperature, internal convection is the most difficult to estimate accurately. Because the gases involved in heat transfer, are at high temperature and are undergoing rapid physical and chemical changes. Uncertainties regarding the airflow pattern, the state of boundary layer development, and the effective gas temperature make the choice of a realistic model almost arbitrary.

The basic equation for calculation of convection heat transfer is (Bergman *et al.* 2011)

$$C_1 = h(T_s - T_\infty) \quad (11)$$

in which  $C_1$  is convection heat transfer,  $h$  is the heat transfer coefficient,  $T_s$  and  $T_\infty$  are the surface and fluid temperatures, respectively. The most problem of convection heat flux is the determination of heat transfer coefficient. In the absence of more exact data, it is reasonable to assume that some form of the classical heat transfer relation for straight pipes, which use the Reynolds analogy, will hold for conditions inside a liner, provided that the local Nusselt number is consistent with established practice for conditions of extreme turbulence.

One of earlier relations for calculation of Nusselt number leading to calculate the heat transfer coefficient is developed by Dittus and Boelter for smooth pipes (Lienhard and Lenhard 2003).

$$Nu_D = 0.0243 Re_D^{0.8} Pr^{0.4} \quad (12)$$

But this relation is valid for low temperature fully developed flow in range of  $2 \times 10^4 < Re_D < 3 \times 10^4$ ,  $L/D \geq 60$ . So, it is not reasonable for calculation of Nusselt number in silo-type combustion chambers. Lienhard and Lenhard (2003) for high temperature is developed a vastly improved description of forced convection in pipes. He recommended the following equation for the local Nusselt number in fully developed flow in smooth pipes which all fluid properties are evaluated at  $T_a$  (Lienhard and Lenhard 2003).

$$Nu_D = \frac{(f/8) Re_D Pr}{1.07 + 12.7 \sqrt{f/8} (Pr^{2/3} - 1)} \quad (13)$$

where  $10^4 < Re_D < 5 \times 10^6$ ,  $0.5 < Pr < 200$ .

And where the friction factor  $f$  is given by

$$f = \frac{1}{(1.82 \log_{10} Re_D - 1.64)^2} \quad (14)$$

In order to obtain Reynolds number, firstly, the velocity of air in the combustion chamber is determined. In axial-flow compressors, the stage pressure rise is very dependent on the axial flow velocity. To achieve the design pressure ratio in the minimum number of stages, a high axial velocity is essential. In many gas turbines, compressor outlet velocity may reach 170 m/s or higher. It is, of course, impractical to attempt to burn fuels in air flowing at such high velocity. Thus, before combustion can proceed, the air velocity must be greatly reduced, usually to about one-fifth of the compressor outlet velocity. This reduction in velocity is accomplished by fitting a diffuser between the compressor outlet and the upstream end of the liner (Boyce 2012). In this study Reynolds number is obtained assuming a typical combustion chamber axial velocity of 30 m/s (Hill and Peterson 1992) and a hydraulic diameter corresponding to the specified combustion chamber diameter of 2.2 m. Near wall convection temperature  $T_a$  is assumed to be similar to average turbine inlet temperature  $T_3$  (Lefebvre 2010), which seems reasonable considering the presence of unmixed air close to the combustor walls that acts as a protection against the flame. Air properties under this near wall temperature are used in the terms of the Eqs. (13)-(14) to calculate heat transfer coefficient  $h_g$ .

### 2.5 Cold side convective heat flux model

In silo-type combustion chambers, compressor supplied air goes through the space between

flame tube and combustor jacket and inter to combustion zone. This passing air, cool the outer metallic shell of flame tube which leads to cooling of backside of ceramic panels.

The Gnielinski correlation of Eq. (9) for lower temperature can be used to estimate the local Nusselt number (Bejan and Kraus 2003).

$$Nu_D = 0.0214(Re_D^{0.8} - 100) Pr^{0.4} \quad (15)$$

In which valid in the range of  $10^4 < Re_D < 5 \times 10^6$ ,  $0.5 < Pr < 1.5$ .

### 2.6 Cold side radiation heat flux model

The amount of radiation heat transferred from the combustion chamber wall to the jacket is usually quite small compared with the external convection heat transfer and at low values that it can often be neglected. For most practical purposes, the following expression based on typical values of emissivity is used as the following form (Lefebvre 2010)

$$R_2 = \varepsilon_{w_2} \sigma (T_{w_2}^4 - T_s^4) \quad (16)$$

### 2.7 Hot and cold side convection

The amount of conduction heat transfer in combustor wall is calculated by Fourier's law which is given by

$$K_{1,2} = -k_{w_{1,2}} \left( \frac{\partial T}{\partial Z} \right) \quad (17)$$

in which  $k_{w_{1,2}}$  is thermal conductivities of the combustor wall and the flame tube outer metallic shell and  $\partial T/\partial Z$  is the temperature gradient in the  $z$ -direction.

Table 2 Hot side radiation calculated and assumed parameters

Parameter	Value
Assumed	
$P_g$ (bar)	11.53
$T_{g_d}$ (K)	1863
$F.A.R$	0.022
$D_i$ (m)	2.2
$\varepsilon_{w_1}$	0.4
Calculated	
$L_m$ (m)	1.32
$\varepsilon_{g_d}$	0.6454
$\varepsilon_{g_p}$	0.5642
$L_g$	1.467

### 2.8 Empirical method

In this method, the liner may be regarded as a container of hot flowing gases surrounded by a casing, with air flowing between the container and the casing. Depending on the geometry and operating conditions, radiation and convection from the hot gases heat up the liner to various extents. The liner is cooled by convection and radiation. At steady state conditions, the rate of heat transfer into a wall must be balanced by the rate of heat transfer out. By assuming equal area on inside and outside of the liner, the basic relation for the heat transfer in the liner can be expressed as Eq. (1). From Lefebvre (2010) for calculation temperature of inner and outer surfaces of combustor wall, Eq. (1) can be rewritten as

$$R_1 + C_1 = R_2 + C_2 = K_1 + K_2 \quad (18)$$

### 3. Temperature distributions in the combustion chamber wall

The Finite Difference Method (FDM) is conducted to predict the temperature distribution of the combustion wall using a MATLAB code.

The general form of heat equation can obtain the temperature distribution  $T(x, y, z)$  is defined as follows

$$\nabla \cdot (k \nabla T) + q = \rho c_p \frac{\partial T}{\partial t} \quad (19)$$

where  $q$  ( $W/m^3$ ),  $c_p$  ( $J/Kg \cdot ^\circ C$ ), and  $\rho$  ( $Kg/m^3$ ) are the heat generated per unit volume, specific heat of material, and density of combustor wall, respectively.  $\nabla T$  in Cartesian coordinates  $(x, y, z)$  is given by:  $\nabla T = \frac{\partial T}{\partial x} \mathbf{i} + \frac{\partial T}{\partial y} \mathbf{j} + \frac{\partial T}{\partial z} \mathbf{k}$ .

Considering three-dimensional (3D) heat transfer for ceramic panel, steady state, no heat generation and the constant thermal conductivity, the Eq. (12) is simplified as follows

$$T_{,xx} + T_{,yy} + T_{,zz} = 0 \quad (20)$$

The finite difference approximation for Eq. (13) at point  $(m, n, k)$  becomes

$$\frac{T_{m+1,n,k} + T_{m-1,n,k} - 2T_{m,n,k}}{(\Delta x)^2} + \frac{T_{m,n-1,k} + T_{m,n+1,k} - 2T_{m,n,k}}{(\Delta y)^2} + \frac{T_{m,n,k+1} + T_{m,n,k-1} - 2T_{m,n,k}}{(\Delta z)^2} = 0 \quad (21)$$

If  $\Delta x \neq \Delta y \neq \Delta z$  then

$$T_{m+1,n,k} + T_{m-1,n,k} + \alpha^2 (T_{m,n+1,k} + T_{m,n-1,k}) + \beta^2 (T_{m,n,k+1} + T_{m,n,k-1}) - 2(1 + \alpha^2 + \beta^2) T_{m,n,k} = 0 \quad (22)$$

where  $\alpha$  and  $\beta$  are the grid aspect ratios

$$\alpha = \frac{\Delta x}{\Delta y} \quad (23)$$

$$\beta = \frac{\Delta x}{\Delta z} \quad (24)$$

Table 3 Hot side convection calculated and assumed parameters

Parameter	Value
Assumed	
$T_a$ (K)	1473
$P_3$ (bar)	9.7
$u_a$ (m/s)	30
$D_h$ (m)	2.2
$\mu \cdot 10^{-5}$ (Kg/m.s)	4.985
Pr	0.705
$K \cdot 10^{-3}$ (w/m.°k)	9.31
Calculated	
$\rho$ (Kg/m <sup>3</sup> )	2.557
$Re_D \cdot 10^6$	2.843
$N_{u_D}$	2512
$h_g$ (w/m.°k)	106

Table 4 Cold side radiation assumed parameters

Parameter	Value
$T_s$ (K)	620
$\epsilon_{w_2}$	0.6

Table 5 Cold side convection calculated and assumed parameters

Parameter	Value
Assumed	
$T_2$ (K)	620
$u_a$ (m/s)	30
$D_h$ (m)	0.264
$\mu \cdot 10^{-5}$ (Kg/m.s)	3.0861
$K \cdot 10^{-3}$ (w/m.°k)	4.77
Calculated	
$\rho$ (Kg/m <sup>3</sup> )	5.461
$Re_D \cdot 10^6$	1.4
$N_{u_D}$	1514
$h_c$ (w/m.°k)	273

#### 4. Results and discussion

The calculated and assumed boundary conditions and parameters for various heat flux models are listed in Tables 2-5. With resulting wall temperatures and heat transfers on both sides (hot and cold sides) for diffusion (luminous) and premix (non-luminous) modes which are calculated and shown in Table 6. Gas emissivity for diffusion and premix modes are provided in Table 2. As can be seen, the gas emissivity of the diffusion mode is more than premix mode. That is why, increasing gas emissivity of the diffusion mode leads to enhance the hot side temperature of the combustor wall and radiation heat flux that this case is more than the premix mode. Comparing values of heat transfers in Table 6, we can observe that convection heat flux at hot side and

Table 6 Hot and cold side calculated temperatures and heat transfers using Eqs. (5)-(11)-(16) to (18)

Diffusion (luminous) mode		Premix (non-luminous) mode	
Parameter	Value	Parameter	Value
$T_{w1}$ (°C)	1100	$T_{w1}$ (°C)	1045
$T_{w2}$ (°C)	960	$T_{w2}$ (°C)	905
$T_{w3}$ (°C)	778	$T_{w3}$ (°C)	743
$R_1$ (Kw/m <sup>2</sup> )	164	$R_1$ (Kw/m <sup>2</sup> )	156
$C_1$ (Kw/m <sup>2</sup> )	-10	$C_1$ (Kw/m <sup>2</sup> )	-16
$R_2$ (Kw/m <sup>2</sup> )	36	$R_2$ (Kw/m <sup>2</sup> )	32
$C_2$ (Kw/m <sup>2</sup> )	118	$C_2$ (Kw/m <sup>2</sup> )	108
$K_1$ (Kw/m <sup>2</sup> )	21	$K_1$ (Kw/m <sup>2</sup> )	21
$K_2$ (Kw/m <sup>2</sup> )	133	$K_2$ (Kw/m <sup>2</sup> )	119

Table 7 Wall temperatures neglecting hot convection and cold radiation

Diffusion mode			Premix mode		
Temperature	Value	Error (%)	Temperature	Value	Error (%)
$T_{w1}$ (°C)	1180	7	$T_{w1}$ (°C)	1140	9
$T_{w2}$ (°C)	1140	8	$T_{w2}$ (°C)	1000	10
$T_{w3}$ (°C)	860	10	$T_{w3}$ (°C)	840	13

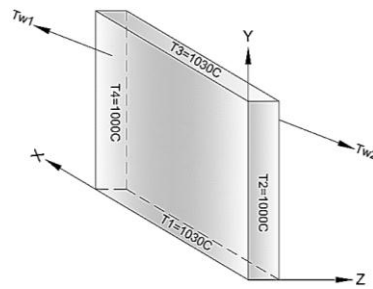


Fig. 6 Boundary temperatures of ceramic panel

radiation heat flux at cold side are less than radiation and convection at the same side, respectively. For this reason, we can neglect them.

Using Table 7, the wall temperatures neglecting hot convection and cold radiation heat transfers are obtained. The relative errors percentage between wall temperatures by considering hot convection and cold radiation heat transfers in Table 6 and wall temperatures without considering hot convection and cold radiation heat transfers in Table 7 are calculated and shown in this Table.

To evaluate temperature distribution using 3D-FDM, in addition to front and rear sides of panel temperatures, the thermal boundary conditions of all other ceramic sides must also be estimated. From field observations, considering passing of dilution air from left and right faces of panel, other boundary temperatures are estimated which are shown in Fig. 6 then employed using a MATLAB code. The finite-difference grid employed here are  $2 \times 2 \times 8$  mm grid nodes in the  $x$ ,  $y$ , and  $z$  directions, respectively. So  $\Delta x = \Delta y = 0.02$  mm,  $\Delta z = 0.008$  mm, namely, each ceramic panel is divided into six layers in the  $z$  direction which the first and the sixth layers are boundary layers and others layers (second, third, fourth, fifth) are mid layers. Fig. 7 shows three-dimensional temperature distribution of ceramic panel using 3D-FDM by MATLAB Code ( $x = y = 0.2$  m,  $z = 0.04$  m) also Figs. 8-11 depict temperature distribution for second, third, fourth and fifth layers of that at  $z = 0.008, 0.016, 0.024, 0.032$  mm at  $xy$  plane, A) 3D-FDM by MATLAB code B) ANSYS software C) ABAQUS software, respectively.

With a view to the Figs. 8-11, two temperature areas are distinguished; center area and lateral area, which there are a good agreement between three computed temperature distributions at these areas. The values of center area temperature are listed in Table 8. Also, we can observe at the first layer (from Fig. 7) as well as at the second and third layers (from Figs. 8-9) the maximum temperature is made at the center area.

Table 8 The center area temperature for 2<sup>nd</sup>, 3<sup>rd</sup>, 4<sup>th</sup>, 5<sup>th</sup> layers

Layer	Temperature (°C)		
	MATLAB	ANSYS	ABAQUSE
2	1072	1077	1068
3	1045	1042	1053
4	1017	1018	1006
5	982	983	991

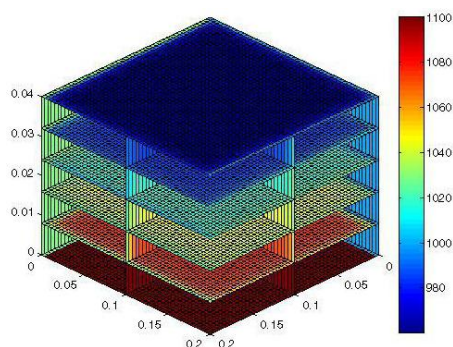


Fig. 7 3-D temperature distribution of ceramic panel

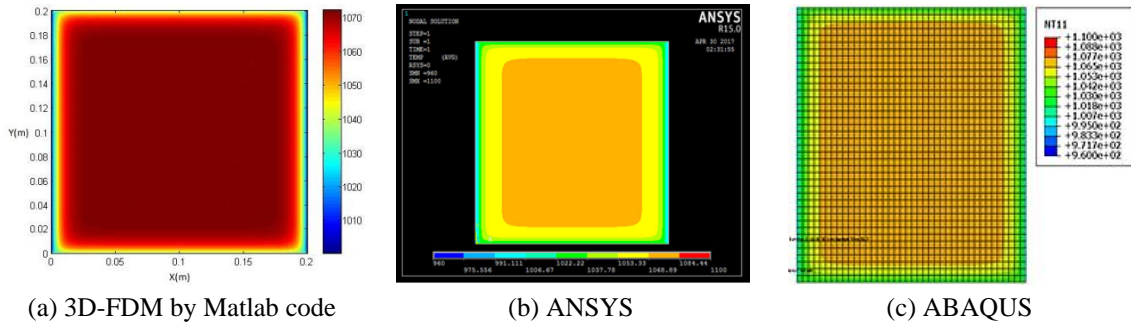


Fig. 8 Temperature distribution for  $z = 0.008$  mm at  $xy$  plane

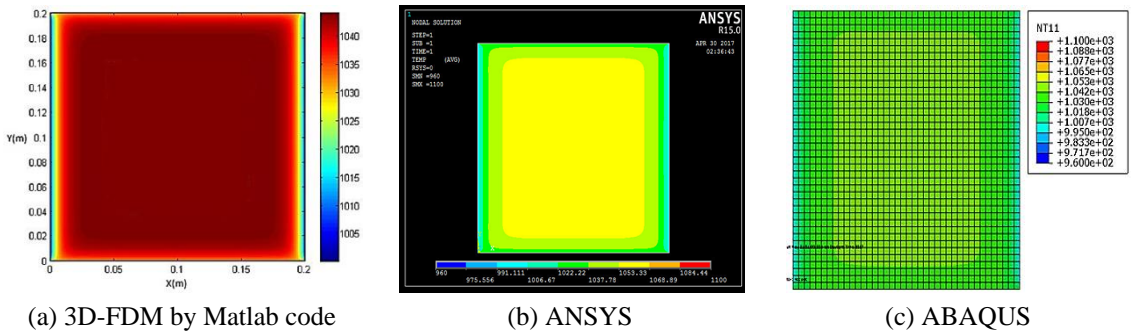


Fig. 9 Temperature distribution for  $z = 0.016$  mm at  $xy$  plan

One of the gas turbine manufacturers provided a reference model to distinguish allowable and not-allowable crack areas which show in Fig. 12. From comparing temperature distribution in layer 2 in Fig. 8 and not-allowable crack area in Fig. 12, we can see clearly, the center area of temperature distribution which has high temperature and high thermal stress, in turn, is match to center area of reference model. Also, at corners of ceramic panel because of concentration of heat fluxes and the change shape, thermal stress is high therefore the risk of crack development in these areas will increase.

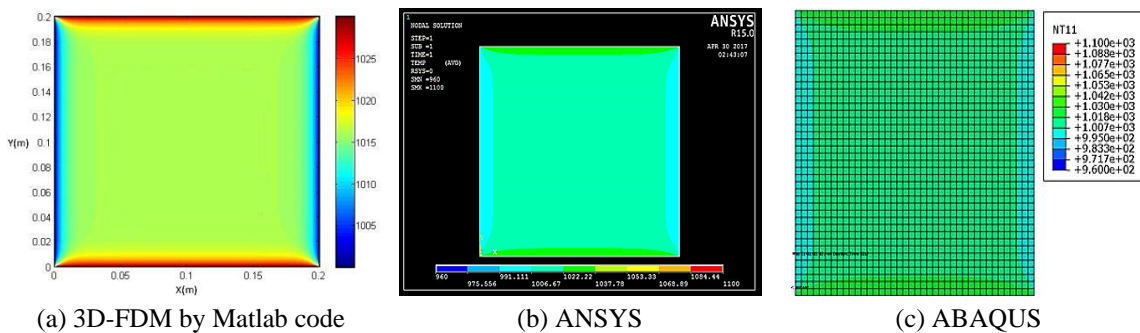


Fig. 10 Temperature distribution for  $z = 0.024$  mm at  $xy$  plane

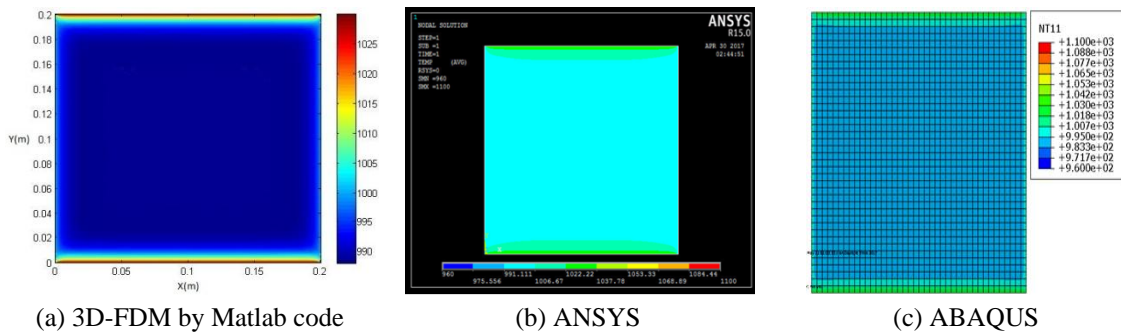
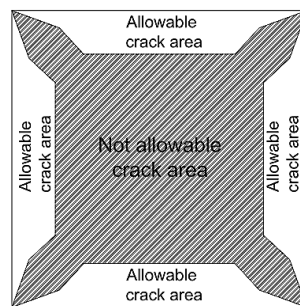
Fig. 11 Temperature distribution for  $z = 0.0032$  mm at  $xy$  plane

Fig. 12 Gas turbine manufacturers allowable and not allowable crack area for V94.2 model

## 5. Conclusions

In this study, the hot and cold side temperatures for a V94.2 gas turbine combustor wall subjected to realistic operation conditions and for diffusion (luminous) and premix (non-luminous) modes is calculated. Also, the radiation, convection and conduction heat transfers at hot and cold side of ceramic panel are calculated. The temperature distribution of ceramic panels is computed using three-dimensional finite difference method (3D-FDM). Results show that the gas emissivity for diffusion mode is more than premix therefore the radiation heat flux and temperature will be more. The radiation heat flux at the hot side of panel and the convection heat flux at the cold side are the effective heat fluxes at combustion chamber wall. Temperature distribution is in such a way that two areas are created, center area and lateral area. There is a good agreement between three computed temperature distributions which by MATLAB, ANSYS and ABAQUS. By comparing values of heat transfers, we can observe that convection heat flux at hot side and radiation heat flux at cold side are much less than radiation and convection at the same side, respectively. For this reason, we can neglect them. The results show that the relative errors percentage between wall temperatures by considering hot convection and cold radiation heat transfers and wall temperatures without considering hot convection and cold radiation heat transfers are less than 10 and 13 for diffusion and premix modes, respectively. Thus, one can neglect the effect of hot convection and cold radiation heat transfers and wall temperatures. From comparing temperature distribution, we can see clearly, the center area of temperature distribution which has high temperature and high thermal stress, in turn, is match to center area of

reference model. Also, at corners of ceramic panel because of concentration of heat fluxes and the change shape, thermal stress is high therefore the risk of crack development in these areas will increase.

## Acknowledgments

The authors would like to thank the referees for their valuable comments. Also, they are thankful to the University of Kashan for supporting this work by Grant No. 682561/1.

## References

- Aditya, K., Gruber, A., Xu, Ch., Lu, T., Krisman, A., Bothien, M.R. and Chen, J.H. (2019), "Direct numerical simulation of flame stabilization assisted by autoignition in a reheat gas turbine combust", *Proceed. Combust. Inst.*, **37**(2), 2635-2642. <https://doi.org/10.1016/j.proci.2018.06.084>
- Andreini, A., Becchi, R., Facchini, B., Picchi, A. and Peschiulli, A. (2017), "The effect of effusion holes inclination angle on the adiabatic film cooling effectiveness in a three-sector gas turbine combustor rig with a realistic swirling flow", *Int. J. Therm. Sci.*, **121**, 75-88. <https://doi.org/10.1016/j.ijthermalsci.2017.07.003>
- Arani, A.G., Hashemian, M., Loghman, A. and Mohammadimehr, M. (2011), "Study of dynamic stability of the double-walled carbon nanotube under axial loading embedded in an elastic medium by the energy method", *J. Appl. Mech. Technical Phys.*, **52**(5), 815-824. <https://doi.org/10.1134/S0021894411050178>
- Arani, A.G., Amir, S., Mozdianfard, M.R., Khoddami Maraghi, Z. and Mohammadimehr, M. (2012a), "Electro-thermal non-local vibration analysis of embedded DWBNNTs", *IMEchE, Part C: J. Mech. Eng. Sci.*, **226**(5), 1410-1422. <https://doi.org/10.1177/0954406211422619>
- Arani, A.G., Mobarakeh, M.R., Shams, Sh. and Mohammadimehr, M. (2012b), "The effect of CNT volume fraction on the magneto-thermo-electro-mechanical behavior of smart nanocomposite cylinder", *J. Mech. Sci. Technol.*, **26**(8), 2565-2572. <https://doi.org/10.1007/s12206-012-0639-5>
- Bejan, A. and Kraus, A.D. (2003), *Heat Transfer Handbook*, John Wiley & Sons, Inc., New Jersey, USA.
- Bergman, T.L., Lavine, A.S., Incropera, F.P. and Dewitt, D.P. (2011), *Fundamentals of Heat and Mass Transfer*, (7th edition), John Wiley & Sons, Inc., NJ, USA.
- Boyce, M.P. (2012), *Gas Turbine Engineering Handbook*, (4<sup>th</sup> edition), Butterworth-Heinemann, Elsevier Inc., NY, USA.
- Bradshaw, S. and Waitz, L. (2006), "Impact of manufacturing variability on combustor liner durability", *J. Eng. Gas Turbines Power*, **131**(3), 032503. <https://doi.org/10.1115/1.2980016>
- Chau, J.L.H., Pan, A. and Yang, Ch. (2017), "Preparation of gas-atomized Fe-based alloy powders and HVOF sprayed coatings", *Adv. Mater. Res., Int. J.*, **6**(4), 343-348. <https://doi.org/10.12989/amr.2017.6.4.343>
- Goodger, E.M. (2007), *Aerospace Fuels*, Landfall Press, Norwich, UK.
- Gustafsson, K.M.B. and Johansson, T. (2001), "An experimental study of surface temperature distribution on effusion-cooled plates", *J. Eng. Gas. Turb. Power.*, **123**, 308-316. <https://doi.org/10.1115/1.1364496>
- Hill, P.G. and Peterson, C.R. (1992), *Mechanics and Thermodynamics of Propulsion*, (2nd edition), Addison- Wesley Inc., Boston, MA, USA.
- Kim, K.M., Yun, N., Jeon, Y.H., Lee, D.H., Cho, H.H. and Kang, S. (2010a), "Conjugated heat transfer and temperature distributions in a gas turbine combustion liner under base-load operation", *J. Mech. Sci. Technol.*, **24**(9), 1939-1946. <https://doi.org/10.1007/s12206-010-0625-8>
- Kim, K.M., Yun, N., Jeon, Y.H., Lee, D.H. and Cho, H.H. (2010b), "Failure analysis in after shell section of gas turbine combustion liner under base-load operation", *Eng. Fail. Anal.*, **17**(4), 848-856.

- <https://doi.org/10.1016/j.engfailanal.2009.10.018>
- Koc, I. (2015), "The use of liquefied petroleum gas (lpg) and natural gas in gas turbine jet engines", *Adv. Energy Res., Int. J.*, **3**(1), 31-43. <https://doi.org/10.12989/eri.2015.3.1.031>
- Lefebvre, A.H. (2010), *Gas Turbine Combustion*, (3rd edition), Taylor and Francis Group, NY, USA.
- Lienhard, J.H. and Lenhard, V.J.H. (2003), *A Heat Transfer Text Book*, (3<sup>rd</sup> edition), Phlogiston Press Cambridge, MA, USA.
- Martiny M., Schulz, A. and Witting, S. (1995), "Full-Coverage Film Cooling Investigations: Adiabatic Wall Temperatures and Flow Visualization", *ASME Conference Proceedings*, Houston, TX, USA.
- Matarazzo, S. and Laget, H. (2011), "Modeling of heat transfer in a gas turbine liner combustor", Chia Laguna, Cagliari, Sardinia, Italy, 11-15.
- Mohammadimehr, M. and Mehrabi, M. (2017), "Stability and free vibration analyses of double-bonded micro composite sandwich cylindrical shells conveying fluid flow", *Appl. Math. Model.*, **47**, 685-709. <https://doi.org/10.1016/j.apm.2017.03.054>
- Mohammadimehr, M. and Mostafavifar, M. (2016), "Free vibration analysis of sandwich plate with a transversely flexible core and FG-CNTs reinforced nanocomposite face sheets subjected to magnetic field and temperature-dependent material properties using SGT", *Compos. Part B*, **94**(1), 253-270. <https://doi.org/10.1016/j.compositesb.2016.03.030>
- Mohammadimehr, M. and Rahmati, A.H. (2013), "Small scale effect on electro-thermo-mechanical vibration analysis of single-walled boron nitride nanorods under electric excitation", *Turkish J. Eng. Environ. Sci.*, **37**, 1-15.
- Mohammadimehr, M., Salemi, M. and Rousta Navi, B. (2016), "Bending, buckling, and free vibration analysis of MSGT microcomposite Reddy plate reinforced by FG-SWCNTs with temperature- dependent material properties under hydro-thermo-mechanical loadings using DQM", *Compos. Struct.*, **138**, 361-380. <https://doi.org/10.1016/j.compstruct.2015.11.055>
- Mohammadimehr, M., BabaAkbar Zarei, A., Parakandeh, A. and Arani, A.G. (2017), "Vibration analysis of double-bonded sandwich microplates with nanocomposite facesheets reinforced by symmetric and un-symmetric distributions of nanotubes under multi physical fields", *Struct. Eng. Mech., Int. J.*, **64**(3), 361-379. <https://doi.org/10.12989/sem.2017.64.3.361>
- Mohammadimehr, M., Atifeh, S.J. and Rousta Navi, B. (2018a), "Stress and free vibration analysis of piezoelectric hollow circular FG-SWBNNNTs reinforced nanocomposite plate based on modified couple stress theory subjected to thermo-mechanical loadings", *J. Vib. Control*, **24**(15), 3471-3486. <https://doi.org/10.1177/1077546317706887>
- Mohammadimehr, M., Emdadi, M., Afshari, H. and Rousta Navi, B. (2018b), "Bending, buckling and vibration analyses of MSGT microcomposite circular-annular sandwich plate under hydro-thermo-magneto-mechanical loadings using DQM", *Int. J. Smart Nano Mater.*, **9**(4), 233-260. <https://doi.org/10.1080/19475411.2017.1377312>
- Mukherji, D., Rosler, J. and Wehrs, J. (2012), "Co-Re-based alloys a new class of material for gas turbine applications at very high temperatures", *Adv. Mater. Res., Int. J.*, **1**(3), 205-219. <https://doi.org/10.12989/amr.2013.1.3.205>
- Najjar, Y.S.H. (2000), "Gas turbine cogeneration systems: a review of some novel cycles", *Appl. Therm. Eng.*, **20**, 179-197. [https://doi.org/10.1016/S1359-4311\(99\)00019-8](https://doi.org/10.1016/S1359-4311(99)00019-8)
- Perpignan, A.A.V., Rao, A.G. and Roekaerts, D.J.E.M. (2018), "Flameless combustion and its potential towards gas turbines", *Prog. Energy. Combust. Sci.*, **69**, 28-62. <https://doi.org/10.1016/j.pecs.2018.06.002>
- Poullikkas, A. (2005), "An overview of current and future sustainable gas turbine technologies", *Renew. Sustain. Energy. Rev.*, **9**(5), 409-443. <https://doi.org/10.1016/j.rser.2004.05.009>
- Rajaei, Gh., Aftabi, F. and Ehyaei, M.A. (2017), "Feasibility of using biogas in a micro turbine for supplying heating, cooling and electricity for a small rural building", *Adv. Energy Res., Int. J.*, **5**(2), 129-145. <https://doi.org/10.12989/eri.2017.5.2.129>
- Sanaye, S., Amani, M. and Amani, P. (2018), "4E modeling and multi-criteria optimization of CCHPW gas turbine plant with inlet air cooling and steam injection", *Sustain. Energy Technol. Assess.*, **29**, 70-81. <https://doi.org/10.1016/j.seta.2018.06.003>

- Sousa, J., Paniagua, G. and Morata, E.C. (2017), "Thermodynamic analysis of a gas turbine engine with a rotating detonation combustor", *Appl. Energy*, **195**, 247-256.  
<https://doi.org/10.1016/j.apenergy.2017.03.045>
- Rahmati, A.H. and Mohammadimehr, M. (2014), "Vibration analysis of non-uniform and non-homogeneous boron nitride nanorods embedded in an elastic medium under combined loadings using DQM", *Physica B: Condensed Matter*, **440**, 88-98. <https://doi.org/10.1016/j.physb.2014.01.036>
- Reeves, D. (1956), "Flame radiation in an industrial gas turbine combustion chamber", *National Gas Turbine Establishment*, NGTE Memo M285, UK.
- Rist, J.F., Dias, M.F., Palman, M., Zalazo, D. and Cukurel, B. (2017), "Economic dispatch of a single micro-gas turbine under CHP operation", *Appl. Energy*, **200**, 1-18.  
<https://doi.org/10.1016/j.apenergy.2017.05.064>
- Rostami, R., Mohammadimehr, M., Ghannad, M. and Jalali, A. (2018), "Forced vibration analysis of nano-composite rotating pressurized microbeam reinforced by CNTs based on MCST with temperature-variable material properties", *Theor. Appl. Mech. Lett.*, **8**, 97-108. <https://doi.org/10.1016/j.taml.2018.02.005>
- TerMaath, C.Y., Skolnik, E.G., Schefer, R.W. and Keller, J.O. (2006), "Emissions reduction benefits from hydrogen addition to midsize gas turbine feedstocks", *Int. J. Hyd. Energy.*, **31**(9), 1147-1158.  
<https://doi.org/10.1016/j.ijhydene.2005.10.002>
- TUGA (2012), V94.2 Gas Turbine Maintenance and Training.
- Wan, H., Gao, Z., Ji, J., Fang, J. and Zhang, Y. (2019), "Experimental study on horizontal gas temperature distribution of two propane diffusion flames impinging on an unconfined ceiling", *Int. J. Therm. Sci.*, **136**, 1-8. <https://doi.org/10.1016/j.ijthermalsci.2018.10.010>
- Wang, X., Wei, K., Tao, Y., Yang, X., Zhou, H., He, R. and Fang, D. (2019), "Thermal protection system integrating insulation materials and multi-layer ceramic matrix composite cellular sandwich panels", *Compos. Struct.*, **209**, 523-534. <https://doi.org/10.1016/j.compstruct.2018.11.004>
- Yang, Z., Adeosun, A., Kumfer, B.B. and Axelbaum, R.L. (2017), "An approach to estimating flame radiation in combustion chambers containing suspended-particles", *Fuel*, **199**, 420-429.  
<https://doi.org/10.1016/j.fuel.2017.02.083>
- Yazdani, R., Mohammadimehr, M. and Roustavi Navi, B. (2019), "Free vibration of Cooper-Naghdi micro saturated porous sandwich cylindrical shells with reinforced CNT face sheets under magneto-hydro-thermo-mechanical loadings", *Struct. Eng. Mech., Int. J.*, **70**(3), 351-365.  
<https://doi.org/10.12989/sem.2019.70.3.351>